A technique to describe the macroscopic pressure dependence of diffusive properties of solid materials containing heterogeneities

T.I. Zohdi [a,*], K. Hutter [b], P. Wriggers [a]

[a] *Institut für Baumechanik und Numerische Mechanik, Appelstrasse 9A, 30167 Hannover, Germany*
[b] *Institut für Mechanik, D-64289 Darmstadt, Germany*

Abstract

In this paper the pressure dependence of macroscopic of "homogenized" diffusive properties of materials containing heterogeneities is investigated. The model involves a pressure dependent regularization of the spatially variable material, by a relation between averages over statistically representative samples subjected to various pressure loadings. The pressure dependence of the local diffusive properties enters through an Arhennius type model. In the regularization process the boundary value problems are posed over the statistically representative samples of material. By definition, such samples contain a large number of heterogeneities, and thus the associated numerical computations require extremely high nodal mesh densities to capture the irregular oscillatory internal fields. In order to simplify the problem, the pressure fields are approximated, above and below in an energetic sense, via classical extremal methods. With these approximations, the pointwise diffusivity coefficients are constructed as a function of pressure. Further approximations are made of the internal geometry by employing a technique of Huet et al. [13]. This allows the use of a Cartesian geometry that can be easily handled with a finite difference scheme. With these approximations, numerical simulations are performed to investigate the regularized macroscopic diffusive properties as a function of macroscopic applied pressure. © 1999 Elsevier Science B.V. All rights reserved.

Keywords: Diffusion; Heterogeneous materials; Coupled fields; Regularization

1. Introduction

The goal of this work is to describe the pressure dependence of macroscopic or "homogenized" diffusive properties of materials containing heterogeneities. There have been a large number of models proposed to describe diffusion, or relatedly, heat conduction, in *homogeneous* media which deviate from the classical models of Fick and Fourier. Works dating back, at least, to Maxwell [17] (1867) have postulated such models. We refer the reader to an extensive survey of virtually all nonstandard models from that of Maxwell through to 1989 found in Joseph and Preziosi [15] for details. There is no shortage of such models, which are generally related to descriptions of thermoelastic coupling, of which specific reviews can be found

---

[*] Corresponding author. E-mail: zohdi@tresca.ifbnm.uni-hannover.de

in Dreyer and Struchtrup [6], Chandrasekhariah [3] and Müller and Ruggeri [18]. In general, such models augment the classical models of Fick and Fourier with terms representing multiple field interaction or higher order effects. Specifically, with regards to the effects of stress on the diffusion of small species through solid media, there is also no shortage of models, of widely varying complexity, and we refer the reader to the classical work of Crank [4] for reviews.

Regardless of the diffusion model, if one were to attempt to perform a direct numerical simulation, say of associated transport phenomena through heterogeneous materials, an extremely fine spatial discretization mesh would be needed to capture the effects of the relatively fine scale heterogeneities (Fig. 1). The resulting system of equations would contain literally billions of numerical unknowns. Such problems are beyond the capacity of computing machines for the foreseeable future. Furthermore, the exact subsurface geometry is virtually impossible to ascertain exactly. Additionally, even if one could solve such a system, the amount of information to process would be of such complexity that it would be difficult to extract any useful data on the desired macroscopic behavior.

It is important to realize that solutions to partial differential equations, even of linear material models, of small structures containing a few heterogeneities are still open problems. Because of these facts, the use of *regularized or homogenized* material properties (resulting in smooth coefficients in the partial differential equations) are commonplace in virtually all branches of physical sciences. The usual approach is to compute a constitutive "relation between averages", relating volume averaged field variables. Thereafter, the regularized properties can be used in a macroscopic analysis (Fig. 2). The volume averaging takes place over a statistically representative sample of material, referred to in the literature as a representative volume element (RVE). The internal fields to be volumetrically averaged must be computed by solving a series of boundary value problems with test loadings posed over the RVE. However, for a sample to be statistically representative it must usually contain a great number of heterogeneities (Fig. 2), and therefore the computations over the RVE are still quite large. However, such computations are manageable on high performance workstations if memory efficient numerical schemes are used. Therefore, while the "RVE problem" must still be solved numerically, it is of reduced computational effort in comparison with a direct attack on the "real" problem. Such regularization processes are referred to in the literature as "homogenization", "mean field theories", "theories of effective properties", etc. The essentials of the theory can be found in Jikov et al. [14]. It is the objective of this paper to apply such averaging techniques to determine stress dependent regularized diffusive properties of the form: $\boldsymbol{D}^{\sigma*}$, where $\langle \boldsymbol{F} \rangle_\Omega = -\boldsymbol{D}^{\sigma*} \cdot \langle \nabla c \rangle_\Omega$ with $\langle \cdot \rangle_\Omega \overset{\text{def}}{=} (1/|\Omega|) \int_\Omega \cdot \, \mathrm{d}\boldsymbol{x}$. In
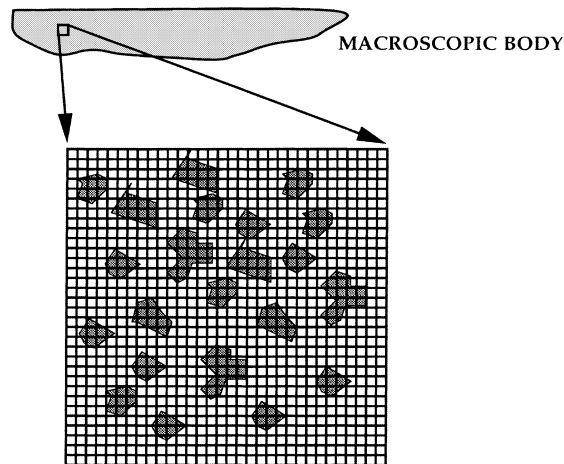

Fig. 1. Fine mesh densities are needed to capture internal length scales.
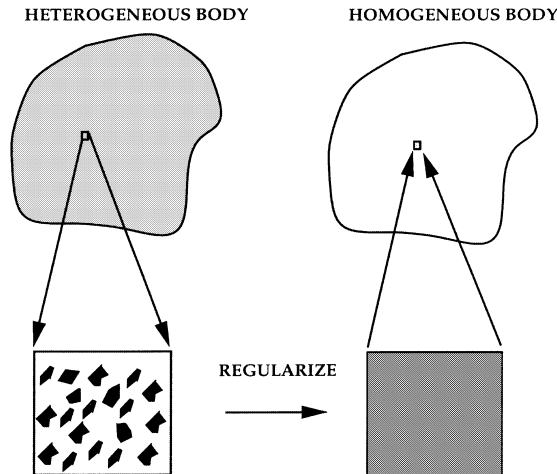
HETEROGENEOUS BODY HOMOGENEOUS BODY

REGULARIZE

Fig. 2. The regularization process. A statistically representative sample of material is extracted and a regularized property is computed. The regularized property is then used in macroscopic calculations.

this definition F and ∇c, which are dependent on the stress fields, are the flux and concentration gradient fields of a solute within the RVE domain Ω. $D^{\sigma*}$ is referred to as a stress dependent effective diffusivity. The goal of the paper is to study the effects of pressure on $D^{\sigma*}$.

One application where the stress sensitivity in solid state diffusion is important, is in the macroscopic depth-dependent diffusive behavior of geological materials, which contain a wide variety of heterogeneities: mineral phases, rock, hollow cavities, biodegradable matter, etc. For example, the permeability of material surrounding underground salt domes, which are used to store oil or hazardous waste products, is of prime importance. Clearly, as one progresses deeper into the subsurface, the heterogeneous material is increasingly pressurized, in a nonuniform way, thus affecting the macroscopic transport characteristics, in particular the diffusive properties (Fig. 3). Another area of interest is in the environmental degradation of metal matrix composites due to the absorption of excessive amounts of hydrogen in combination with residual or applied tensile stresses. In general it is believed that hydrogen damage in metallic materials occurs because of excessive hydrogen absorption in regions of high tensile stress triaxiality which lowers the

HETEROGENEITIES

SURFACE LEVEL

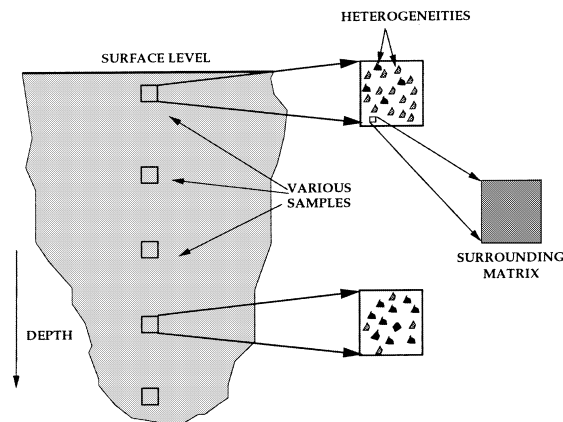VARIOUS
SAMPLES

SURROUNDING
MATRIX

DEPTH

Fig. 3. One application: samples extracted at various depths within a geological layer, having varying effective diffusivities due to changes in pressure.

surface energy required for intergranular micro-cracks to grow. Loosely speaking, hydrogen sufficiently reduces the bonding energy of the metal lattice enough to allow intergranular cracking or "decohesion". There are numerous works in the area of granular decohesion, and we refer the reader to Gerberich et al. [7–9]. The important effect is that the grains are observed to decohese, and that the likelihood of decohesion is directly related to the amount of hydrogen present. Hydrogen is attracted to regions of high negative pressure, and vice versa. Roughly speaking, in both of the mentioned applications, one can naively think of the microstructure as being "opened up" or "closed down", allowing preferential, and non-preferential, diffusive regions. We refer the reader to continuum models, which have attempted to relate the effects of stress on diffusivity in the context of hydrogen damage: Aifantis [1], Doig and Jones [5], Unger et al. [20,21] and Zohdi and Meletis [22]. Common to all of these models is the implicit incorporation of the pressure into the diffusive constitutive law. In this paper we use a relatively simple pressure dependent model on the "microscale", which has been mathematically investigated in Zohdi and Wriggers [23], to describe the local diffusive behavior. This model is employed within an RVE in conjunction with the regularization process described. The model involves a pressure dependent regularization of the spatially variable material, by a relation between averages over statistically representative samples subjected to various pressure loading. The pressure dependence of the local diffusive properties enters through an Arhennius type model. The modeling embeds the effects of microstress field into an otherwise ordinary diffusivity tensor.

The outline of the paper is as follows. In Section 2 the governing equations for the coupled fields are introduced. In Section 3 bounding fields are used to approximate the pressure field, thus focusing the computations on the diffusive part. In Section 4 a method of approximating the heterogeneous geometry with a Cartesian one is presented. The Cartesian geometry is handled with a memory efficient finite difference scheme to allow the computations to proceed quickly on a single workstation. In Section 5 numerical experiments are then carried out simulating the response of macroscopic materials with applied pressure. In Section 6 concluding remarks are given.

2. Governing equations

We consider a structure which occupies an open bounded domain in $\Omega \in \mathbb{R}^3$. Its boundary is denoted $\partial\Omega$, and consists of a portion Γ_c and a part Γ_f, where the concentrations ($c = d$, d specified) and fluxes ($\boldsymbol{F} \cdot \boldsymbol{n} = q$, q specified, $\boldsymbol{n}$ = outward normal) are applied, respectively. All quantities are functions of space unless explicitly stated otherwise. To model steady state stress/diffusion interaction, a relatively uncomplicated approach is to embed stress dependency directly into the diffusivity tensor

$$-\nabla \cdot \boldsymbol{F} = 0, \quad \boldsymbol{F} = -\boldsymbol{D}^\sigma(\boldsymbol{\sigma}) \cdot \nabla_c, \tag{1}$$

where c is the concentration of the solute, $\boldsymbol{\sigma}$ is the Cauchy stress present at a point, and $\boldsymbol{D}^\sigma$ is a positive definite, spatially variable, second order tensorial function of position. The stress fields will be approximated by bounding techniques later, and can be considered as a given tensorial field. It is well-known that the diffusivity of a material is pressure and temperature dependent, and can be postulated in the following Arhennius form at a point $\boldsymbol{x}$ (see Ref. [20] for example)

$$\boldsymbol{D}^\sigma = \boldsymbol{D}^0 \mathrm{e}^{-(Q(p)/R\theta)}, \tag{2}$$

where $\boldsymbol{D}^0$ is a spatially heterogeneous diffusivity tensor at absolute zero degrees Kelvin and $Q(P)$ is the pressure dependent activation energy for solute motion per mole of diffusive species. Here $P = -\mathrm{tr}\,\boldsymbol{\sigma}/3$ is the pressure (tr = trace), θ is the absolute temperature and R is the universal gas constant. We approximate the activation energy by a constant times the dilatation (volumetric) strain energy leading to

$$Q(P) \approx \frac{\alpha}{2} \frac{\mathrm{tr}\,\boldsymbol{\sigma}}{3} \frac{\mathrm{tr}\,\boldsymbol{\epsilon}}{3}, \tag{3}$$

where the stress fields are governed by

$$\nabla \cdot \boldsymbol{\sigma} = \mathbf{0}, \quad \boldsymbol{\sigma} = \boldsymbol{E} : \boldsymbol{\epsilon}, \quad \boldsymbol{\epsilon} \stackrel{\text{def}}{=} \frac{\nabla \boldsymbol{u} + (\nabla \boldsymbol{u})^T}{2}, \tag{4}$$

where $\boldsymbol{E}$ is a spatially variable symmetric, positive definite fourth rank linear elasticity tensor, and $\boldsymbol{u}$ is the displacement field. If $\boldsymbol{E}$ is isotropic, then $P = -(\operatorname{tr} \boldsymbol{\sigma}/3) = -3\kappa(\operatorname{tr} \boldsymbol{\epsilon}/3)$, where κ is the bulk modulus. This leads to an approximation for the pressure-dependent diffusivity,

$$Q(P) \approx \frac{\alpha}{2} \frac{\operatorname{tr} \boldsymbol{\sigma}}{3} \frac{\operatorname{tr} \boldsymbol{\epsilon}}{3} = \frac{\alpha}{2} \frac{P^2}{3\kappa} \Rightarrow \boldsymbol{D}^\sigma = \boldsymbol{D}^0 \exp\left(-\frac{\frac{\alpha}{2} \frac{P^2}{3\kappa}}{R\theta} \right) \stackrel{\text{def}}{=} \boldsymbol{D}^0 \exp\left(-\gamma \frac{P^2}{3\kappa} \right), \tag{5}$$

where $\gamma \stackrel{\text{def}}{=} \alpha/2R\theta$. We ignore deviatoric (distortional) effects. α is a material constant which can be measured with ordinary experimental techniques. We refer the reader to Haasen [10] or Stark [19] for discussions. Essentially this involves standard tests for determining diffusivity constants, however with samples under pressure (see Ref. [22]).

3. Pressure approximations

In this paper the pressure fields will be approximated, above and below in a certain sense. Thereafter, we can construct the local pressure dependent diffusive coefficients throughout the body. In order to approximate the pressure fields we employ standard micro/macro energy arguments. Usually, macroscopic, aggregate or "effective" constitutive relations of a micro-heterogeneous material are computed from a relation between averaged stress and strain in a statistically RVE with volume $|\Omega|$. Typically one determines $\boldsymbol{E}^*$, where $\langle \boldsymbol{\sigma} \rangle_\Omega = \boldsymbol{E}^* : \langle \boldsymbol{\epsilon} \rangle_\Omega$. In this definition $\boldsymbol{\sigma}$ and $\boldsymbol{\epsilon}$ are the stress and strain fields within the domain Ω. However, for the relation between averages to make sense, i.e., to be statistically representative, the sample size may have to be quite large relative to the intrinsic length scales of the microstructure. The size requirements placed on the RVE can be stated concisely by the following micro/macro energy equality, $\langle \boldsymbol{\sigma} : \boldsymbol{\epsilon} \rangle_\Omega = \langle \boldsymbol{\sigma} \rangle_\Omega : \langle \boldsymbol{\epsilon} \rangle_\Omega$, known as Hill's condition [11]. For a heterogeneous body, two important loadings that fall under Hill's condition are:

$$
\begin{aligned}
&(1) \ \boldsymbol{u}|_{\partial\Omega} = \boldsymbol{S} \cdot \boldsymbol{x} \Rightarrow \langle \boldsymbol{\epsilon} \rangle_\Omega = \boldsymbol{S}, \\
&(2) \ \boldsymbol{t}|_{\partial\Omega} = \boldsymbol{T} \cdot \boldsymbol{n} \Rightarrow \langle \boldsymbol{\sigma} \rangle_\Omega = \boldsymbol{T},
\end{aligned}
\tag{6}
$$

where $\boldsymbol{S}$ and $\boldsymbol{T}$ are constant strain and stress tensors, respectively. Clearly, for Hill's condition to be realizable in a sample within a macroscopic structure under possibly nonuniform external loading, the sample must be large enough to have negligibly small field fluctuations relative to its size. Under Hill's condition it is possible to relate $\boldsymbol{E}^*$ to the approximations $\langle \boldsymbol{E} \rangle_\Omega$, $\langle \boldsymbol{E}^{-1} \rangle_\Omega^{-1}$ due to classical Voigt (constant strain throughout the body) and Reuss (constant stress throughout the body), respectively. As a simple calculation reveals $\langle \boldsymbol{\sigma} : \boldsymbol{\epsilon} \rangle_\Omega = \langle \boldsymbol{\sigma} \rangle_\Omega : \langle \boldsymbol{\epsilon} \rangle_\Omega$ implies $\langle \boldsymbol{E}^{-1} \rangle_\Omega^{-1} \leqslant \boldsymbol{E}^* \leqslant \langle \boldsymbol{E} \rangle_\Omega$. As is well known, one can relate the upper bound to an assumed constant strain (Voigt) field within the RVE, $\boldsymbol{\epsilon} = \boldsymbol{c}$

$$\langle \boldsymbol{\sigma} \rangle_\Omega = \langle \boldsymbol{E} : \boldsymbol{\epsilon} \rangle_\Omega = \langle \boldsymbol{E} \rangle_\Omega : \boldsymbol{c} \Rightarrow \boldsymbol{E}^* = \langle \boldsymbol{E} \rangle_\Omega. \tag{7}$$

Alternatively, an assumed constant stress (Reuss) field, $\boldsymbol{\sigma} = \boldsymbol{k}$ yields

$$\langle \boldsymbol{\epsilon} \rangle_\Omega = \langle \boldsymbol{E}^{-1} : \boldsymbol{\sigma} \rangle_\Omega = \langle \boldsymbol{E}^{-1} \rangle_\Omega : \boldsymbol{k} \Rightarrow \boldsymbol{E}^* = \langle \boldsymbol{E}^{-1} \rangle_\Omega^{-1}. \tag{8}$$

Therefore, the Reuss and Voigt fields provide the two extremes of possible elastic microfield behavior. The first produces kinematically inadmissible fields, while the second produces statically inadmissible fields. We will use these extreme conditions to construct the approximations to the pressure fields.
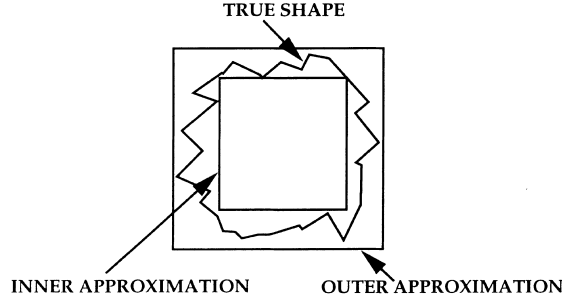
Fig. 4. The approximation by simple shapes by the Hill modification theorem.

3.1. Construction of approximate local diffusivities

The Reuss and Voigt approximations, along with the results in Eq. (6), allow the following approximations for the pressure fields

$$
\begin{aligned}
\text{Reuss}: P &= -\kappa \frac{\operatorname{tr} \epsilon}{3} = \text{constant}, \\
\text{Voigt}: \frac{\operatorname{tr} \epsilon}{3} &= -\frac{P}{\kappa} = \text{constant}.
\end{aligned}
\tag{9}
$$

We assume uniform pressure loading (justified for a large sample) on the boundary, denoted P^0,

$$
\boldsymbol{\sigma} \cdot \boldsymbol{n}|_{\partial\Omega} = \begin{bmatrix} \pm P^0 & 0 & 0 \\ 0 & \pm P^0 & 0 \\ 0 & 0 & \pm P^0 \end{bmatrix} \begin{bmatrix} n_1 \\ n_2 \\ n_3 \end{bmatrix}.
\tag{10}
$$

Therefore, we have for the Reuss uniform stress approximation

$$
\text{Reuss}: P = -\kappa \frac{\operatorname{tr} \epsilon}{3} = P^0 \Rightarrow \boldsymbol{D}^{\sigma R} \stackrel{\text{def}}{=} \boldsymbol{D}^0 \exp\left(-\gamma \frac{(P^0)^2}{3\kappa} \right),
\tag{11}
$$

Table 1
Local material property values used in the simulations. For simplicity, the diffusivities, which are solute dependent, were taken to be inversely proportional to the densities: $1/\rho$ (kg/m^3) $= D^0$ (m/s^2)

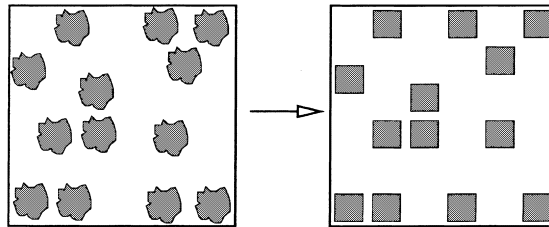| Material	Density: ρ (kg/m^3)	κ (GPa)	D^0 (m/s^2)	γ (n/m)
Matrix	1000	10	1000×10^{-6}	1×10^{-7}
Hard	5000	20	200×10^{-6}	1×10^{-7}
Soft	200	2	5000×10^{-6}	1×10^{-7}

Fig. 5. The heterogeneous internal material structure approximated by the Hill modification theorem.
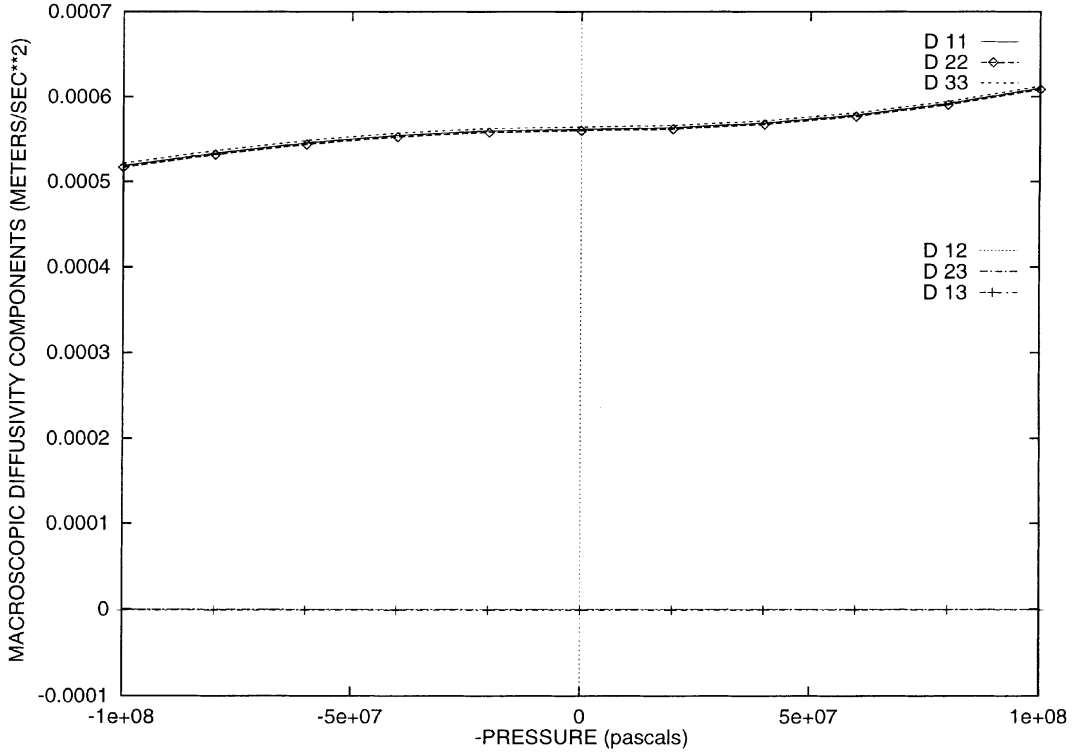
Fig. 6. 72.6%-matrix/27.4%-hard: the behavior of the effective diffusivity tensor components with variations in pressure, where the approximate Reuss field was used to construct the activation energy.

and for the Voigt uniform strain approximation

$$\text{Voigt}: \left\langle \kappa \frac{\text{tr } \epsilon}{3} \right\rangle_\Omega = \langle \kappa \rangle_\Omega \frac{\text{tr } \epsilon}{3} = -P^0 \Rightarrow \frac{\text{tr } \epsilon}{3} = \frac{-P^0}{\langle \kappa \rangle_\Omega} \Rightarrow P = \kappa \frac{P^0}{\langle \kappa \rangle_\Omega} \Rightarrow \boldsymbol{D}^{\sigma V} \overset{\text{def}}{=} \boldsymbol{D}^0 \exp\left(-\gamma \frac{\left(\kappa \frac{P^0}{\langle \kappa \rangle_\Omega} \right)^2}{3\kappa} \right),$$
(12)

where we used the fact that $\langle P \rangle_\Omega = P^0$, as implied by Eq. (6). By directly comparing the exponents in the approximate representation of the diffusion coefficients, we have the following *locally valid* observations

$$\text{If } \kappa > \langle \kappa \rangle_\Omega : \qquad \underbrace{\boldsymbol{D}^0 \exp\left(-\gamma \frac{(P^0)^2}{3\kappa} \right)}_{\text{constructed with Reuss pressure}} \quad < \quad \underbrace{\boldsymbol{D}^0 \exp\left(-\gamma \frac{\left(\kappa \frac{P^0}{\langle \kappa \rangle_\Omega} \right)^2}{3\kappa} \right)}_{\text{constructed with Voigt pressure}} \quad ,$$

$$\text{If } \kappa < \langle \kappa \rangle_\Omega : \qquad \underbrace{\boldsymbol{D}^0 \exp\left(-\gamma \frac{(P^0)^2}{3\kappa} \right)}_{\text{constructed with Reuss pressure}} \quad > \quad \underbrace{\boldsymbol{D}^0 \exp\left(-\gamma \frac{\left(\kappa \frac{P^0}{\langle \kappa \rangle_\Omega} \right)^2}{3\kappa} \right)}_{\text{constructed with Voigt pressure}} \quad .$$
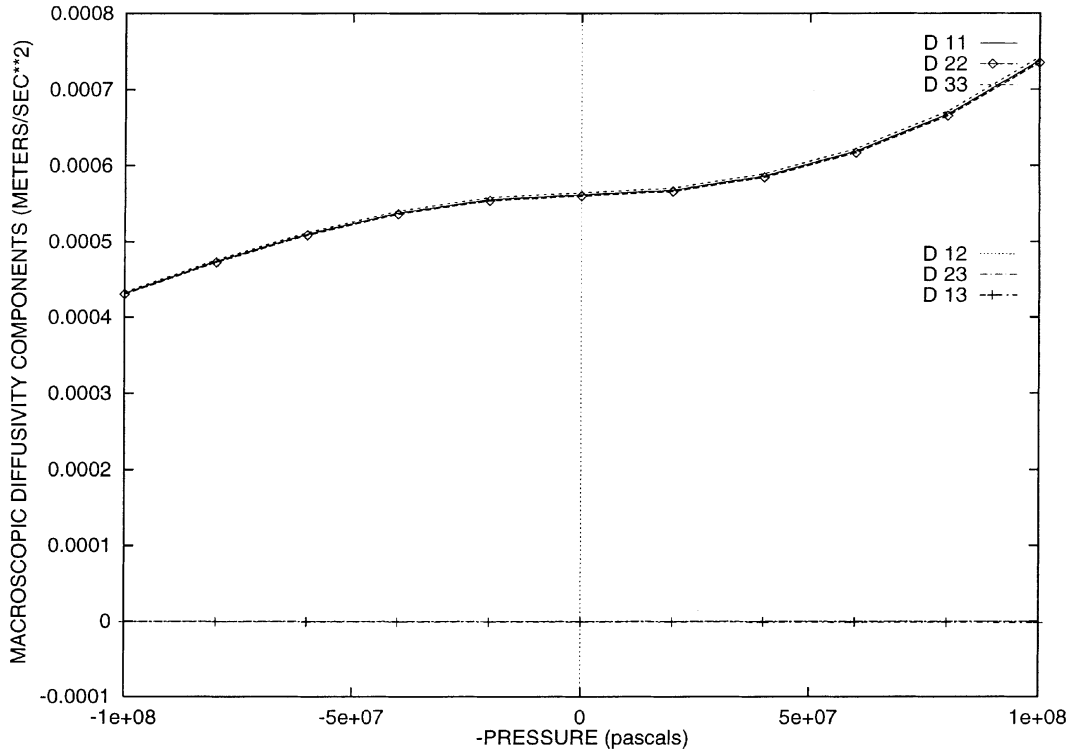(13)

Fig. 7. 72.6%-matrix/27.4%-hard: the behavior of the effective diffusivity tensor components with variations in pressure, where the approximate Voigt field was used to construct the activation energy.

Clearly if a matrix material possess a larger volume fraction in a sample, and if it is of higher diffusivity, the Voigt pressure approximation produces a larger effective diffusivity.

Similar to the case of effective elastic properties, in order to determine an effective macroscopic linear diffusivity tensor, $\boldsymbol{D}^{\sigma*}$, $\langle \boldsymbol{F} \rangle_\Omega = -\boldsymbol{D}^{\sigma*} \cdot \langle \nabla c \rangle_\Omega$, must be computed, where $\boldsymbol{F}$ and ∇c are the flux and concentration gradient fields within a statistically RVE with volume $|\Omega|$. The Hill–Reuss–Voigt bounds apply trivially to determine bounds on stress-dependent effective properties for each approximate pressure field. However, because the global diffusive properties are our primary objectives, we need more accuracy than simply bounds on them. However, the bounds on each approximate diffusivity construction can be computed analytically, and provide some qualitative behavior for $\boldsymbol{D}^{\sigma*}$. They are as follows:

Bounds for the Reuss pressure construction:

$$\left\langle \left(\boldsymbol{D} \exp\left(-\gamma \frac{(P^0)^2}{3\kappa} \right) \right)^{-1} \right\rangle_\Omega^{-1} \leqslant \boldsymbol{D}^{\sigma R*} \leqslant \left\langle \boldsymbol{D}^0 \exp\left(-\gamma \frac{(P^0)^2}{3\kappa} \right) \right\rangle_\Omega,$$

Bounds for the Voigt pressure construction:

$$\left\langle \left(\boldsymbol{D}^0 \exp\left(-\gamma \frac{\left(\kappa \frac{P^0}{\langle \kappa \rangle_\Omega} \right)^2}{3\kappa} \right) \right)^{-1} \right\rangle_\Omega^{-1} \leqslant \boldsymbol{D}^{\sigma V*} \leqslant \left\langle \boldsymbol{D}^0 \exp\left(-\gamma \frac{\left(\kappa \frac{P^0}{\langle \kappa \rangle_\Omega} \right)^2}{3\kappa} \right) \right\rangle_\Omega .$$
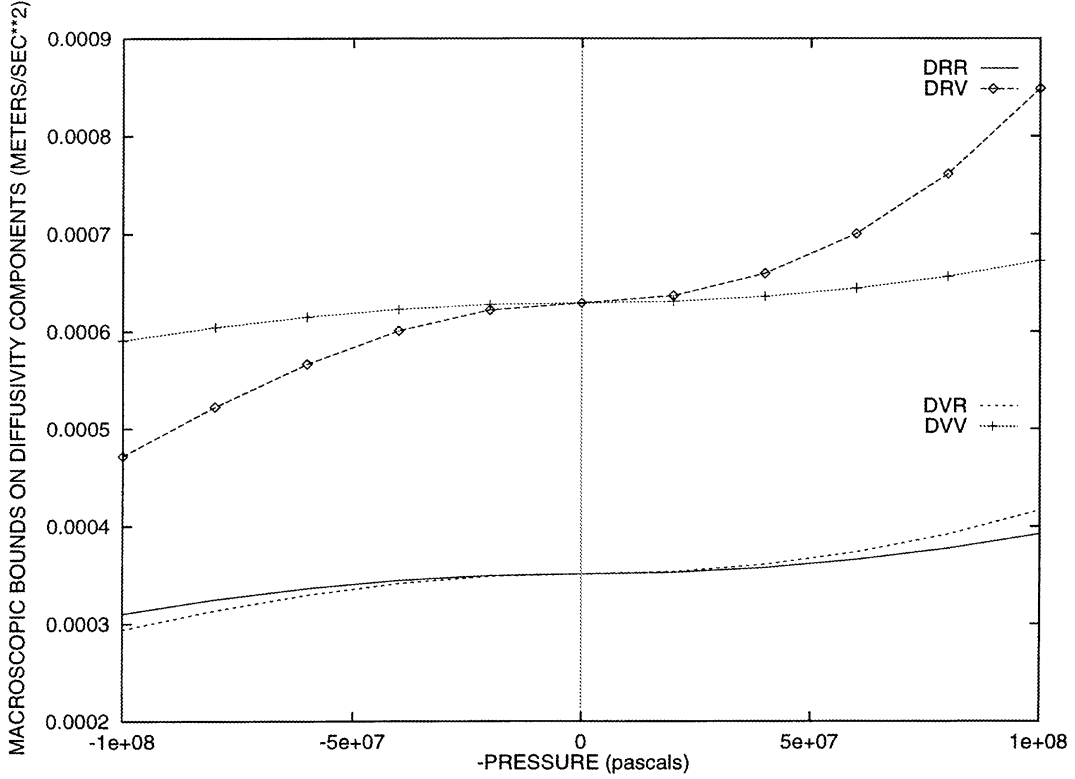
(14)

Fig. 8. 72.6%-matrix/27.4%-hard: the behavior of the effective diffusivity tensor components with variations in pressure. The diffusive Reuss/Voigt bounds for the Reuss and Voigt pressure constructions: $\text{DRR} \overset{\text{def}}{=} \langle (D^{\sigma R})^{-1} \rangle^{-1}$, $\text{DRV} \overset{\text{def}}{=} \langle D^{\sigma R} \rangle$, $\text{DVR} \overset{\text{def}}{=} \langle (D^{\sigma V})^{-1} \rangle^{-1}$ and $\text{DVV} \overset{\text{def}}{=} \langle D^{\sigma V} \rangle$.

4. Computational testing procedure

Our approach is to (1) approximate the pressure fields by Reuss, and then the Voigt pressure fields, (2) construct the local pressure-dependent diffusive properties for both cases, and (3) to directly compute $\boldsymbol{D}^{\sigma*}$ numerically, for both cases. Explicitly, to determine $\boldsymbol{D}^{\sigma*}$, we specify three linearly independent diffusive loadings of the form, (1) $c|_{\partial\Omega} = \boldsymbol{\psi} \cdot \boldsymbol{x} \Rightarrow \langle \nabla c \rangle_{\Omega} = \boldsymbol{\psi}$ or (2) $q|_{\partial\Omega} = \boldsymbol{\beta} \cdot \boldsymbol{n} \Rightarrow \langle \boldsymbol{F} \rangle_{\Omega} = \boldsymbol{\beta}$, where $\boldsymbol{\psi}$ and $\boldsymbol{\beta}$ are prescribed constant vectors. Each independent loading state provides three equations, for a total of nine, which are used to determine the tensor relation between averages, i.e., the regularized "effective" diffusive property (for a given pressure field construction):

$$\begin{bmatrix} -\langle \boldsymbol{F}_1 \rangle_{\Omega} \\ -\langle \boldsymbol{F}_2 \rangle_{\Omega} \\ -\langle \boldsymbol{F}_3 \rangle_{\Omega} \end{bmatrix} = \begin{bmatrix} D^{\sigma*}_{11} & D^{\sigma*}_{12} & D^{\sigma*}_{13} \\ D^{\sigma*}_{21} & D^{\sigma*}_{22} & D^{\sigma*}_{23} \\ D^{\sigma*}_{31} & D^{\sigma*}_{32} & D^{\sigma*}_{33} \end{bmatrix} \begin{bmatrix} \langle (\nabla c)_1 \rangle_{\Omega} \\ \langle (\nabla c)_2 \rangle_{\Omega} \\ \langle (\nabla c)_3 \rangle_{\Omega} \end{bmatrix}. \tag{15}$$

The usual choices for the three independent load cases I, II and III are

$$\boldsymbol{\psi}^{(\text{I}\to\text{III})} \text{ or } \boldsymbol{\beta}^{(\text{I}\to\text{III})} = \begin{bmatrix} \varDelta \\ 0 \\ 0 \end{bmatrix}, \begin{bmatrix} 0 \\ \varDelta \\ 0 \end{bmatrix}, \begin{bmatrix} 0 \\ 0 \\ \varDelta \end{bmatrix}, \tag{16}$$
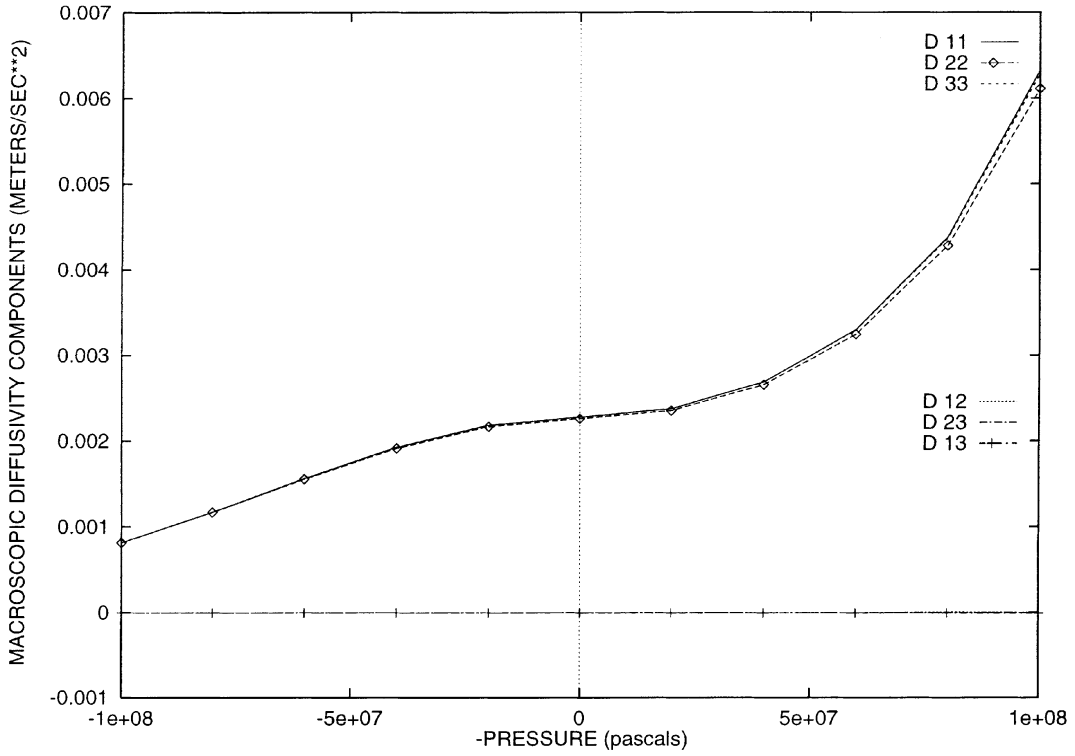
Fig. 9. 72.6%-matrix/27.4%-soft: the behavior of the effective diffusivity tensor components with variations in pressure, where the approximate Reuss field was used to construct the activation energy.

where Δ is a diffusive load parameter. However, we must perform the simulations twice, once for an assumed Voigt field, and once for the assumed Reuss field. We note that $\boldsymbol{D}^{\sigma*}$ is symmetric and positive definite.

4.1. Geometrical approximations by employing the Hill modification theorem

Obviously were one to directly simulate an RVE's response with the exact heterogeneous geometrical shapes, which are quite irregular, a problem of such complexity would occur that virtually no analytical, semi-analytical or standard numerical technique would suffice. Fortunately, for the goal of effective property determination, the shapes can be approximated by much simpler geometries, which is the subject of this section. Our objective is to show that the macroscopic effective response for irregularly shaped particles can be approximated by substituting easier shapes as shown in Fig. 4. This approach has been developed by Huet et al. [13], and is based on the results of Hill [12]. In order to do this, we employ a weak form of a general diffusion equation with diffusivity $\boldsymbol{D}$.

$$\text{Find } c, c|_{\Gamma_c} = d, \text{ such that}$$
$$\int_{\Omega} \nabla v \cdot \boldsymbol{D} \cdot \nabla c \, \mathrm{d}x = \int_{\Gamma_f} v \boldsymbol{F} \cdot \boldsymbol{n} \, \mathrm{d}x \quad \forall v, \ v|_{\Gamma_c} = 0. \tag{17}$$

where $c|_{\Gamma_c} = d$ is the specified concentration boundary data. We use this weak formulation to provide results guiding the use of approximate internal geometries.

Consider two symmetric positive definite material property distributions, $\mathbf{M}_{\mathrm{I}}(\mathbf{x})$ and $\mathbf{M}_{\mathrm{II}}(\mathbf{x})$. Defining, $\delta\nabla c = \nabla c^{\mathrm{II}} - \nabla c^{\mathrm{I}}$ (a "kinematically admissible" test function), we have

$$2W_{\mathrm{I}} \stackrel{\mathrm{def}}{=} \int_{\Omega} \nabla c^{\mathrm{I}} \cdot \mathbf{M}_{\mathrm{I}} \cdot \nabla c^{\mathrm{I}} \, \mathrm{d}\mathbf{x}, \qquad 2W_{\mathrm{II}} \stackrel{\mathrm{def}}{=} \int_{\Omega} (\nabla c^{\mathrm{I}} + \delta\nabla c) \cdot \mathbf{M}_{\mathrm{II}} \cdot (\nabla c^{\mathrm{I}} + \delta\nabla c) \, \mathrm{d}\mathbf{x}. \tag{18}$$

Therefore by direct expansion,

$$
\begin{aligned}
2W_{\mathrm{I}} - 2W_{\mathrm{II}} &= \int_{\Omega} \nabla c^{\mathrm{I}} \cdot \mathbf{M}_{\mathrm{I}} \cdot \nabla c^{\mathrm{I}} \, \mathrm{d}\mathbf{x} - \int_{\Omega} \nabla c^{\mathrm{I}} \cdot \mathbf{M}_{\mathrm{II}} \cdot (\nabla c^{\mathrm{I}} + \delta\nabla c) \mathrm{d}\mathbf{x} \\
&\quad - \underbrace{\int_{\Omega} \delta\nabla c \cdot \mathbf{M}_{\mathrm{II}} \cdot (\nabla c^{\mathrm{I}} + \delta\nabla c) \mathrm{d}\mathbf{x}}_{=\mathbf{0} \ \ \text{if} \ \ \Gamma_c = \partial\Omega} \\
&= \int_{\Omega} \nabla c^{\mathrm{I}} \cdot (\mathbf{M}_{\mathrm{I}} - \mathbf{M}_{\mathrm{II}}) \cdot \nabla c^{\mathrm{I}} \, \mathrm{d}\mathbf{x} - \int_{\Omega} \nabla c^{\mathrm{I}} \cdot \mathbf{M}_{\mathrm{II}} \cdot \delta\nabla c \, \mathrm{d}\mathbf{x} \\
&= \int_{\Omega} \nabla c^{\mathrm{I}} \cdot (\mathbf{M}_{\mathrm{I}} - \mathbf{M}_{\mathrm{II}}) \cdot \nabla c^{\mathrm{I}} \, \mathrm{d}\mathbf{x} - \underbrace{\int_{\Omega} (\nabla c^{\mathrm{I}} + \delta\nabla c) \cdot \mathbf{M}_{\mathrm{II}} \cdot \delta\nabla c \, \mathrm{d}\mathbf{x}}_{=\mathbf{0} \ \ \text{if} \ \ \Gamma_c = \partial\Omega} \\
&\quad + \int_{\Omega} \delta\nabla c \cdot \mathbf{M}_{\mathrm{II}} \cdot \delta\nabla c \, \mathrm{d}\mathbf{x} \\
&= \underbrace{\int_{\Omega} \nabla c^{\mathrm{I}} \cdot (\mathbf{M}_{\mathrm{I}} - \mathbf{M}_{\mathrm{II}}) \cdot \nabla c^{\mathrm{I}} \, \mathrm{d}\mathbf{x}}_{\text{pos.def.for } (\mathbf{M}_{\mathrm{I}} - \mathbf{M}_{\mathrm{II}}) > 0 \ \ \forall\mathbf{x}} + \underbrace{\int_{\Omega} \delta\nabla c \cdot \mathbf{M}_{\mathrm{II}} \cdot \delta\nabla c \, \mathrm{d}\mathbf{x}}_{> 0}.
\end{aligned}
\tag{19}
$$

The vanishing terms are due to a direct application of virtual work. Therefore,

$$(\mathbf{M}_{\mathrm{I}} - \mathbf{M}_{\mathrm{II}}) > \mathbf{0} \Rightarrow \int_{\Omega} \nabla c^{\mathrm{I}} \cdot \mathbf{M}_{\mathrm{I}} \cdot \nabla c^{\mathrm{I}} \, \mathrm{d}\mathbf{x} - \int_{\Omega} (\nabla c^{\mathrm{I}} + \delta\nabla c) \cdot \mathbf{M}_{\mathrm{II}} \cdot (\nabla c^{\mathrm{I}} + \delta\nabla c) \, \mathrm{d}\mathbf{x} > 0. \tag{20}$$

This result does not require uniform loading on the boundary. However, under the special case of uniform test boundary loading, we have

$$\text{If} \ \ c|_{\partial\Omega} = \boldsymbol{\psi} \cdot \mathbf{x} \ \ \text{and} \ \ \mathbf{M}_{\mathrm{I}} - \mathbf{M}_{\mathrm{II}} \geqslant \mathbf{0} \Rightarrow 2W_{\mathrm{I}} - 2W_{\mathrm{II}} = \boldsymbol{\psi} \cdot (\mathbf{M}_{\mathrm{I}}^* - \mathbf{M}_{\mathrm{II}}^*) \cdot \boldsymbol{\psi} |\Omega| \geqslant 0. \tag{21}$$

Therefore if we assign $\mathbf{M}_{\mathrm{II}}$ to be the real microstructure $\mathbf{D}$ composed of irregular shapes, and assign $\mathbf{M}_{\mathrm{I}} = \mathbf{D}^+$ to be the simpler larger shapes that contain the irregular shapes, and compute the corresponding effective property $\mathbf{D}^{*+}$ (see Fig. 4), we have

$$\mathbf{D}^+ - \mathbf{D} \geqslant \mathbf{0}, \quad \forall\mathbf{x} \in \Omega \Rightarrow \mathbf{D}^* \leqslant \mathbf{D}^{*+}. \tag{22}$$

Alternatively, if we assign $\mathbf{M}_{\mathrm{I}}$ to be the real microstructure $\mathbf{D}$ composed of irregular shapes, and assign $\mathbf{M}_{\mathrm{II}} = \mathbf{D}^-$ to be the simpler larger shapes that contain the irregular shapes, and compute the corresponding effective property $\mathbf{D}^{*-}$ (see Fig. 4), we have

$$\mathbf{D} - \mathbf{D}^- \geqslant \mathbf{0}, \quad \forall\mathbf{x} \in \Omega \Rightarrow \mathbf{D}^{*-} \leqslant \mathbf{D}^*. \tag{23}$$
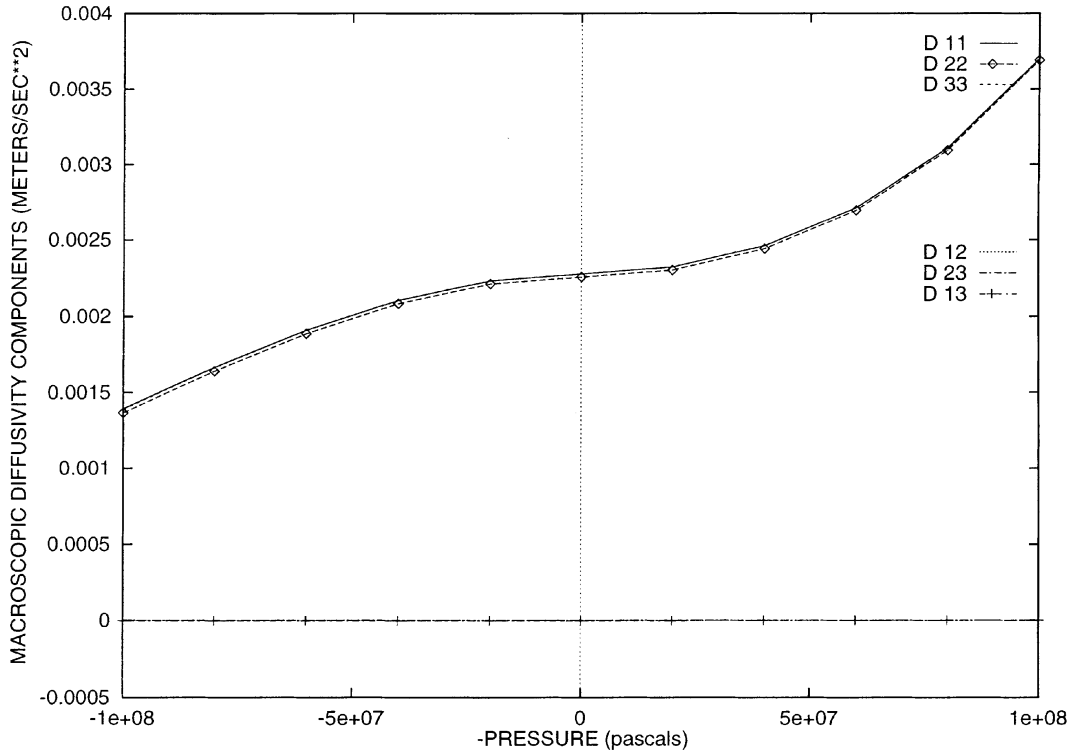
Fig. 10. 72.6%-matrix/27.4%-matrix: the behavior of the effective diffusivity tensor components with variations in pressure, where the approximate Voigt field was used to construct the activation energy.

Therefore we have in total

$$\underbrace{\boldsymbol{D}^{*-}}_{\text{using simpler smaller shapes}} \leqslant \boldsymbol{D}^* \leqslant \underbrace{\boldsymbol{D}^{*+}}_{\text{using simpler larger shapes}}. \tag{24}$$

This motivates the use of relatively simple shapes, such as cubes or spheres, to approximate the true complicated geometries. *However, this is adequate only for the effective macroscopic response.* The results in Eq. (21) are known as the Hill modification theorem. They were first derived by Hill in 1963 [12] for uniform boundary conditions, and have been used extensively by Huet et al. [13] to analyze more complicated microstructures by combining simpler ones. The extensions and proofs for nonuniform boundary conditions (Eq. (20)), in the context of elasticity, were presented in Zohdi and Wriggers [24]. We use the approach to approximate microstructures by cubical particles. The Cartesian geometry allows the use of relatively simple numerical methods, in particular the finite difference method. This is discussed next.

4.2. Taking advantage of the Cartesian geometry

The approximation of the geometry by cubical shapes is highly advantageous from a computational point of view. Using cubical approximations of the heterogeneities permits the use of the finite difference scheme to compute the transport diffusive behavior within the sample. We assume that $\boldsymbol{D}^\sigma$ is pointwise isotropic, but spatially variable. Therefore, $\boldsymbol{D}^\sigma$ can be represented by a scalar function, D^σ times $\boldsymbol{I}$. Using a
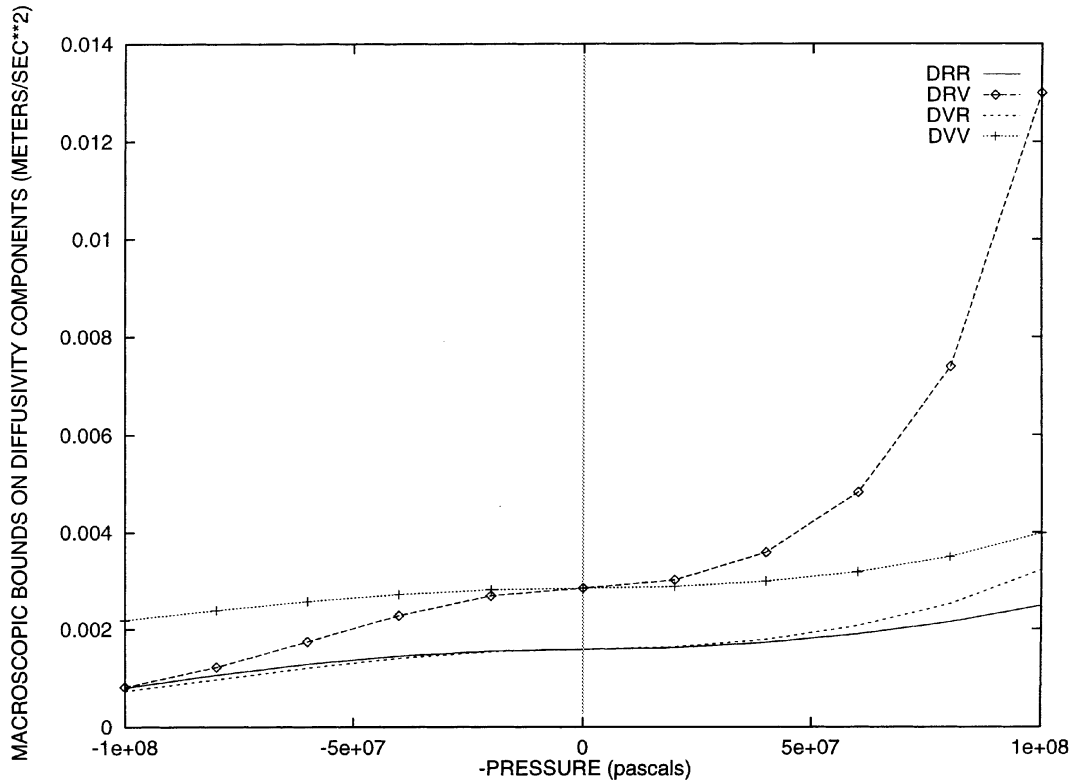
Fig. 11. 72.6%-matrix/27.4%-soft: the behavior of the effective diffusivity tensor components with variations in pressure. The diffusive Reuss/Voigt bounds for the Reuss and Voigt pressure constructions: $\text{DRR} \stackrel{\text{def}}{=} \langle (D^{\sigma R})^{-1} \rangle^{-1}$, $\text{DRV} \stackrel{\text{def}}{=} \langle D^{\sigma R} \rangle$, $\text{DVR} \stackrel{\text{def}}{=} \langle (D^{\sigma V})^{-1} \rangle^{-1}$ and $\text{DVV} \stackrel{\text{def}}{=} \langle D^{\sigma V} \rangle$.

seven point finite difference stencil in three dimensions, the terms that appear in the governing differential equation are approximated as follows

$$
D^\sigma \nabla c \approx D^\sigma(x,y,z) \left(\frac{c(x+h,y,z) - c(x-h,y,z)}{2h} \boldsymbol{i} + \frac{c(x,y+h,z) - c(x,y-h,z)}{2h} \boldsymbol{j} \right.
$$
$$
\left. + \frac{c(x,y,z+h) - c(x,y,z-h)}{2h} \boldsymbol{k} \right), \tag{25}
$$

where h is the uniform grid spacing for the x, y and z directions. Applying the difference formulas once again to the fluxes, we obtain

Table 2
Local material property values used in the "geological" simulations. For simplicity, the diffusivities, which are solute dependent, were taken to be inversely proportional to the densities: $1/\rho$ (kg/m^3) $= D^0$ (m/s^2)

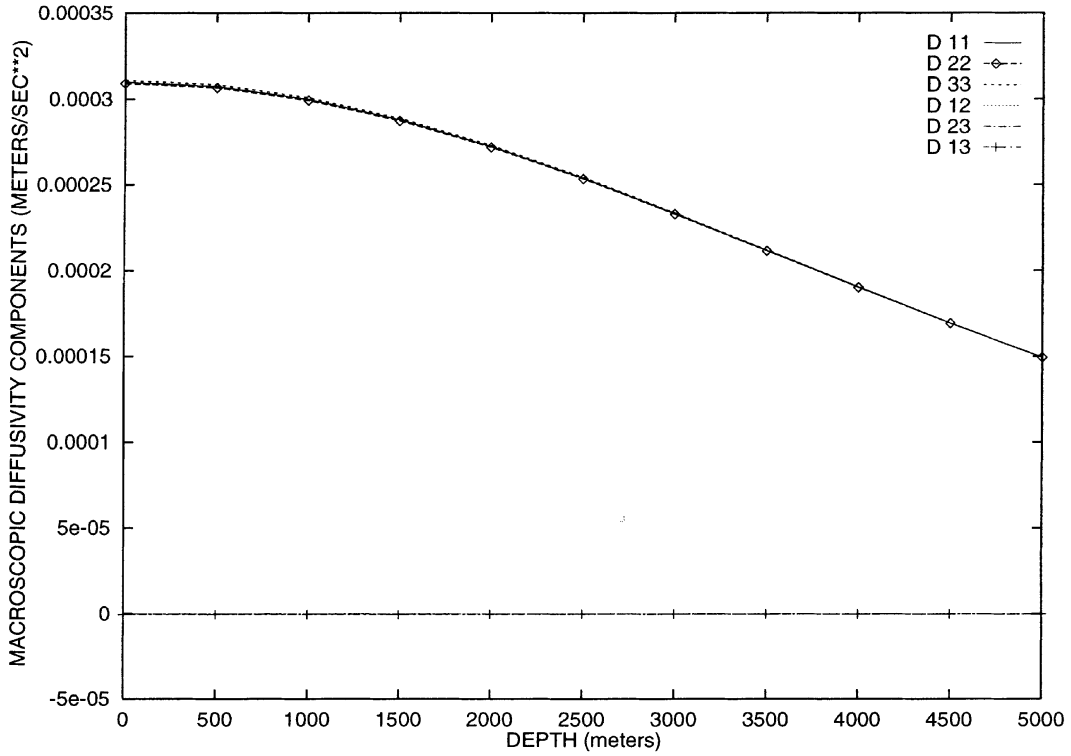| Material	Density: ρ (kg/m^3)	κ (GPa)	D^0 (m/s^2)	γ (n/m)
"Soil"	1920	30.2	520.83×10^{-6}	1×10^{-6}
Iron	7690	162.46	130.04×10^{-6}	1×10^{-8}

Fig. 12. 72.6%-matrix/27.4%-iron: the behavior of the effective diffusivity tensor components with depth, where the approximate Reuss field was used to construct the activation energy.

$$\nabla \cdot (D^\sigma \nabla c) \approx \frac{1}{4h^2} (D^\sigma(x+h,y,z)c(x+2h,y,z) - D^\sigma(x-h,y,z)c(x,y,z)$$

$$- D^\sigma(x+h,y,z)c(x,y,z) + D^\sigma(x-h,y,z)c(x-2h,y,z)$$

$$+ D^\sigma(x,y+h,z)c(x,y+2h,z) - D^\sigma(x,y-h,z)c(x,y,z)$$

$$- D^\sigma(x,y+h,z)c(x,y,z) + D^\sigma(x,y-h,z)c(x,y-2h,z)$$

$$+ D^\sigma(x,y,z+h)c(x,y,z+2h) - D^\sigma(x,y,z-h)c(x,y,z)$$

$$- D^\sigma(x,y,z+h)c(x,y,z) + D^\sigma(x,y,z-h)c(x,y,z-2h)).$$

(26)

Due to the microstructure the numerical mesh density must be quite high for sufficient accuracy. Because of this fact, such simulations typically require a minimum of several thousand degrees of freedom even for a relatively small problem. Such a system of equations must be solved repeatedly. Therefore, computational efficiency and memory is important to allow such problems to be solved on a workstation in a reasonable amount of time. We use a successive over relaxation (SOR) system solver, which permits no matrix storage in the iteration process and is thus has relatively low memory requirements. This approach is classical (see Ref. [2] for example).
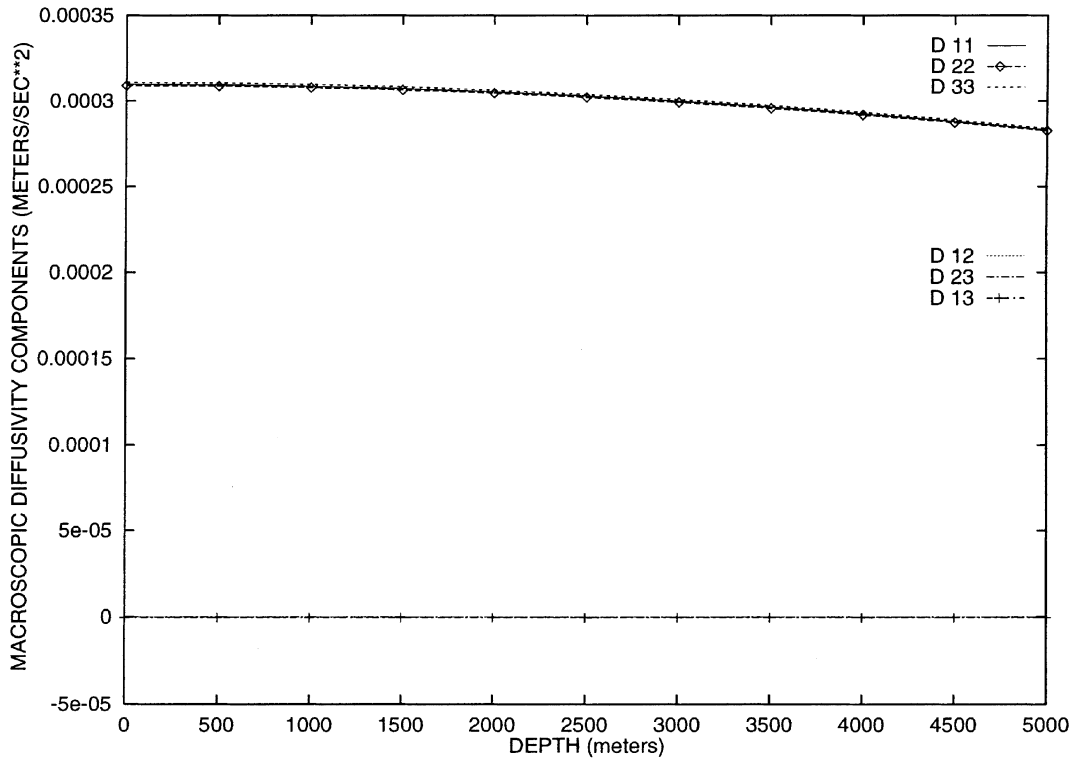
Fig. 13. 72.6%-matrix/27.4%-iron: the behavior of the effective diffusivity tensor components with depth, where the approximate Voigt field was used to construct the activation energy.

5. Numerical experiments

In order to minimize the number of simulations, but illustrate the general behavior of the model, we first tested the values in Table 1. For each computational test, a heterogeneous two-phase material was generated by partitioning a cubical sample into cubical subdomains, and randomly assigning either of the material values until the appropriate volume fractions were achieved. The cubes were shrunk down in the process to allow gaps between the particles (Fig. 5). The volume fraction of the cubical particles was chosen to reflect the volume fraction of the irregular material that would be truly present in the sample. The use of the relatively easy cubical shapes was justified by the analysis of the last section (the Hill modification theorem). The pressures were incremented in steps of 20 MPa, from 100 to −100 MPa. In the tests, we enlarged the sample until we found a certain size, containing enough particles, which provided a stable effective response. In other words, samples above this size produced the same effective diffusive properties. We found a sample size containing 100 cubical particles occupying 27% of the volume was adequately representative for the variety of material combinations tested. The finite difference meshes were repeatedly refined during the testing process until for each experiment, the computed effective properties exhibited no more changes, from mesh to successive mesh, to 5 significant digits. For these tests, a mesh density of $38 \times 38 \times 38$, for a total of 54 872 numerical unknowns/per test was sufficient. This mesh density was used for all final simulation tests. Studying Figs. 6–11, it is clear that the effect is stronger in tension, and was consistently more pronounced with the Reuss construction for the pressure, due to the presence of the more severe term $1/\kappa$, compared to the milder $\kappa/\langle\kappa\rangle_\Omega^2$ term in the Voigt approximation. Also presented in the plots were the Reuss/Voigt diffusive bounds for each approximate pressure construction (see Eq. (14)):
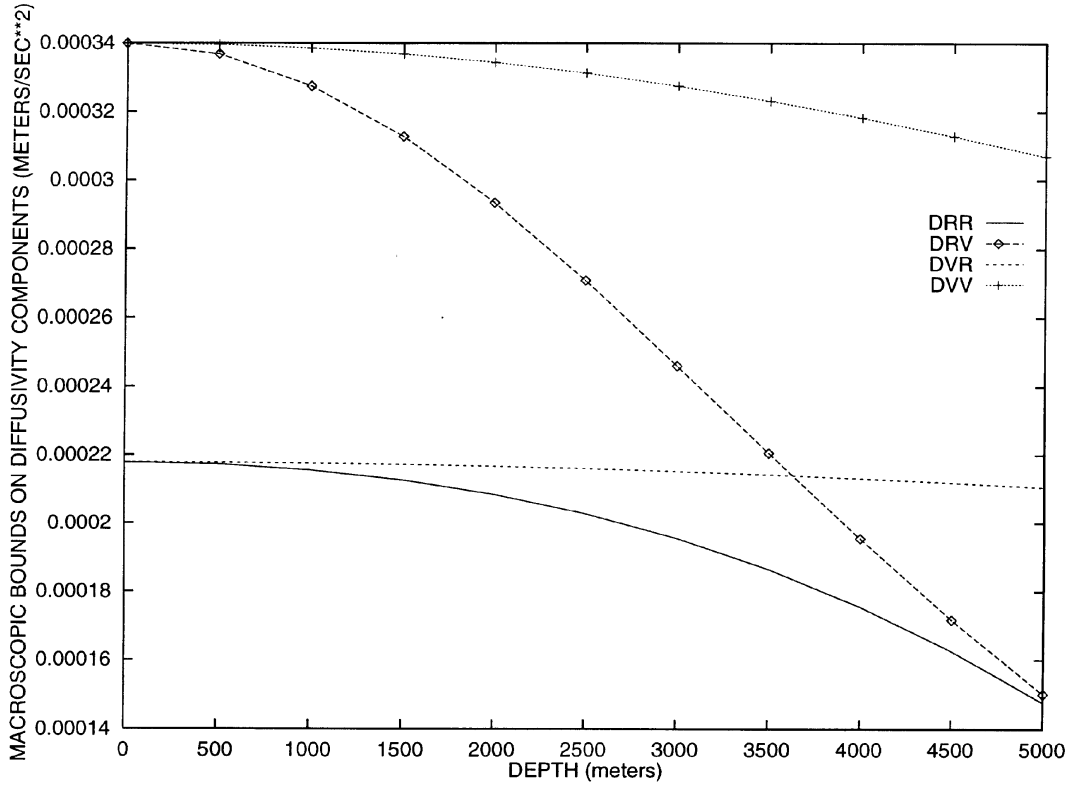
Fig. 14. 72.6%-matrix/27.4%-iron: the behavior of the effective diffusivity tensor components with depth. The diffusive Reuss/Voigt bounds for the Reuss and Voigt pressure constructions: DRR $\stackrel{\text{def}}{=} \langle (D^{\sigma R})^{-1} \rangle^{-1}$, DRV $\stackrel{\text{def}}{=} \langle D^{\sigma R} \rangle$, DVR $\stackrel{\text{def}}{=} \langle (D^{\sigma V})^{-1} \rangle^{-1}$ and DVV $\stackrel{\text{def}}{=} \langle D^{\sigma V} \rangle$.

$$
\langle (\boldsymbol{D}^{\sigma R})^{-1} \rangle_\sigma^{-1} \stackrel{\text{def}}{=} \left\langle \left(\boldsymbol{D}^0 \exp\left(-\gamma \frac{(P^0)^2}{3\kappa} \right) \right)^{-1} \right\rangle_\Omega^{-1}, \quad \boldsymbol{D}^0 = D^0 \boldsymbol{I},
$$

$$
\langle (\boldsymbol{D}^{\sigma R}) \rangle_\sigma \stackrel{\text{def}}{=} \left\langle \boldsymbol{D}^0 \exp\left(-\gamma \frac{(P^0)^2}{3\kappa} \right) \right\rangle_\Omega,
$$

$$
\langle (\boldsymbol{D}^{\sigma V})^{-1} \rangle_\Omega^{-1} \stackrel{\text{def}}{=} \left\langle \left(\boldsymbol{D}^0 \exp\left(-\gamma \frac{\left(\kappa \frac{P^0}{\langle \kappa \rangle_\Omega} \right)^2}{3\kappa} \right) \right)^{-1} \right\rangle_\Omega^{-1}, \tag{27}
$$

$$
\langle \boldsymbol{D}^{\sigma V} \rangle_\Omega \stackrel{\text{def}}{=} \left\langle \boldsymbol{D}^0 \exp\left(-\gamma \frac{\left(\kappa \frac{P^0}{\langle \kappa \rangle_\Omega} \right)^2}{3\kappa} \right) \right\rangle_\Omega.
$$

These bounds gave coarse, but qualitatively correct, behavior of the effective diffusivity with increasing pressure. The computed results always remained within the appropriate theoretical bounds (Figs. 8 and 11). It is clear that at zero pressure the corresponding bounds should collapse together since $\boldsymbol{D}^{\sigma V} = \boldsymbol{D}^{\sigma R}$. In other words, instead of two lower and two upper bounds, there was only one of each at zero pressure.

Table 3
Local material property values used in the "metallurgical" simulations. For simplicity, the diffusivities, which are solute dependent, were taken to be inversely proportional to the densities: $1/\rho$ (kg/m^3) $= D^0$ (m/s^2)

Material	Density: ρ (kg/m^3)	κ (GPa)	D^0 (m/s^2)	γ (n/m)
Aluminum	2700	77.9	370.370×10^{-6}	1×10^{-6}
Titanium carbide	5150	306.6	194.175×10^{-6}	1×10^{-8}

5.1. "Geological" applications

As an application to geological problems we considered depth-dependent sampling. The heterogeneous internal structure is the same as in the previous examples. The testing procedure was to isolate the sample at a given depth, which dictated the ambient pressure loading by the weight of the heterogeneous material above the sample, using the average density $(\langle \rho(x) \rangle_\Omega)$, and to perform the three tests necessary to determine the effective diffusivity for that depth. The depth was increased from 0 to 5000 m, in increments of 500 m. The matrix phase was selected to be "soil" in the simulations (Table 2). The soil properties were specifically those of fused silica. The application we had in mind was related to storage of hazardous waste, and estimation of leakage, in underground salt domes. The local sensitivities to the pressure, γ, were selected to reflect that the soil, when compacted, was relatively more sensitive, by a factor of 100 times (in this example), than the embedded particulate material (iron ore in this example). The results are shown in Figs. 12–14. The effective diffusivities are much more sensitive with the Reuss pressure field than for the Voigt pressure field. This is consistent with the predictions in Eq. (13).
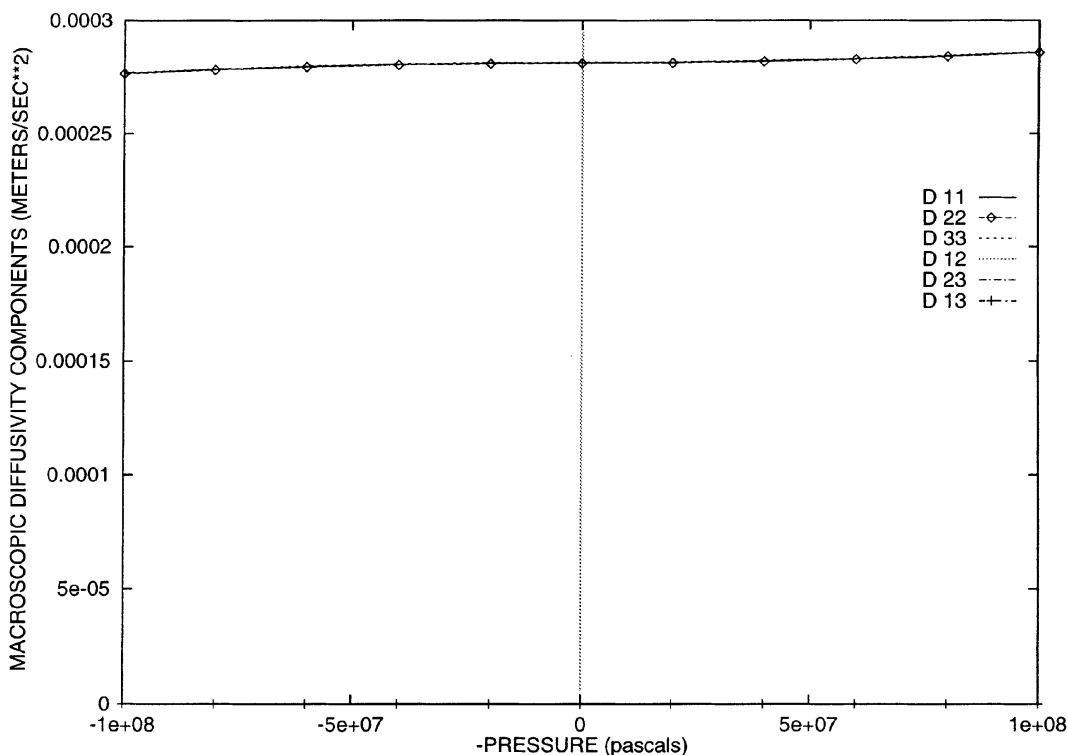

Fig. 15. 72.6%-ALUMINUM/27.4%-TITANIUM CARBIDE: The behavior of the effective diffusivity tensor components with pressure, where the approximate Reuss field was used to construct the activation energy.
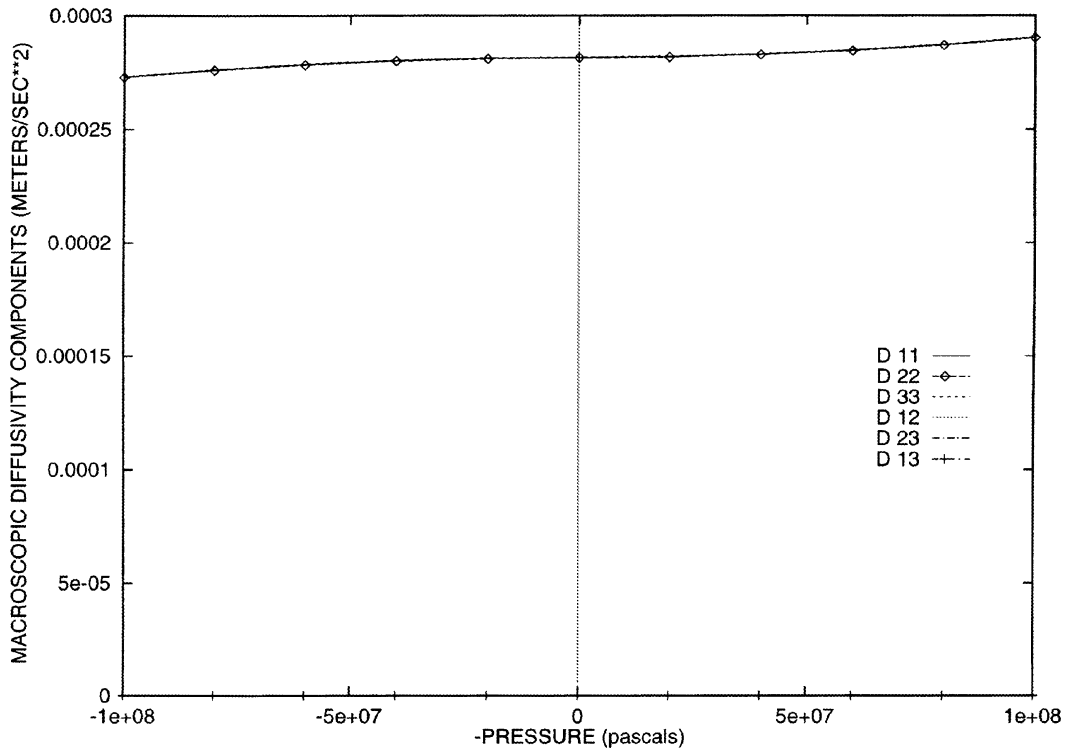
Fig. 16. 72.6%-ALUMINUM/27.4%-TITANIUM CARBIDE: The behavior of the effective diffusivity tensor components with pressure, where the approximate Voigt field was used to construct the activation energy.

5.2. Metallic composite applications

The application to metallic composites was straightforward. We considered an aluminum matrix material with particulate stiffeners of titanium carbide. Combinations of this sort are relatively common. The material values are shown in Table 3. The results are shown in Figs. 15–17. It is clear that the pressure effect is relatively negligible for this combination of material parameters and loading.

6. Conclusions

We have attempted to account for pressure dependent transport properties with the simplest of models. The presented results have provided some initial qualitative information which we intend to use in the development of more advanced models. It is obvious that below the sample length scale level, models describing geometrically large deformations must be employed to capture processes such as pore growth and collapse as a function of pressure. Also, as discussed in Mangeney et al. [16], rate effects can play a critical role for certain types of materials encountered in geological applications, for example ice. The incorporation of both behaviors, and others, into the pressure dependent framework discussed in this paper, is a subject of current work by the authors. Finally, more accurate models, and better characterization of the internal geometries, require more sophisticated numerical approaches. Of primary importance is the more accurate description of the internal stress fields, which are used to construct the diffusivity coefficients. From this point of view, integral based methods, such as the finite element method are more
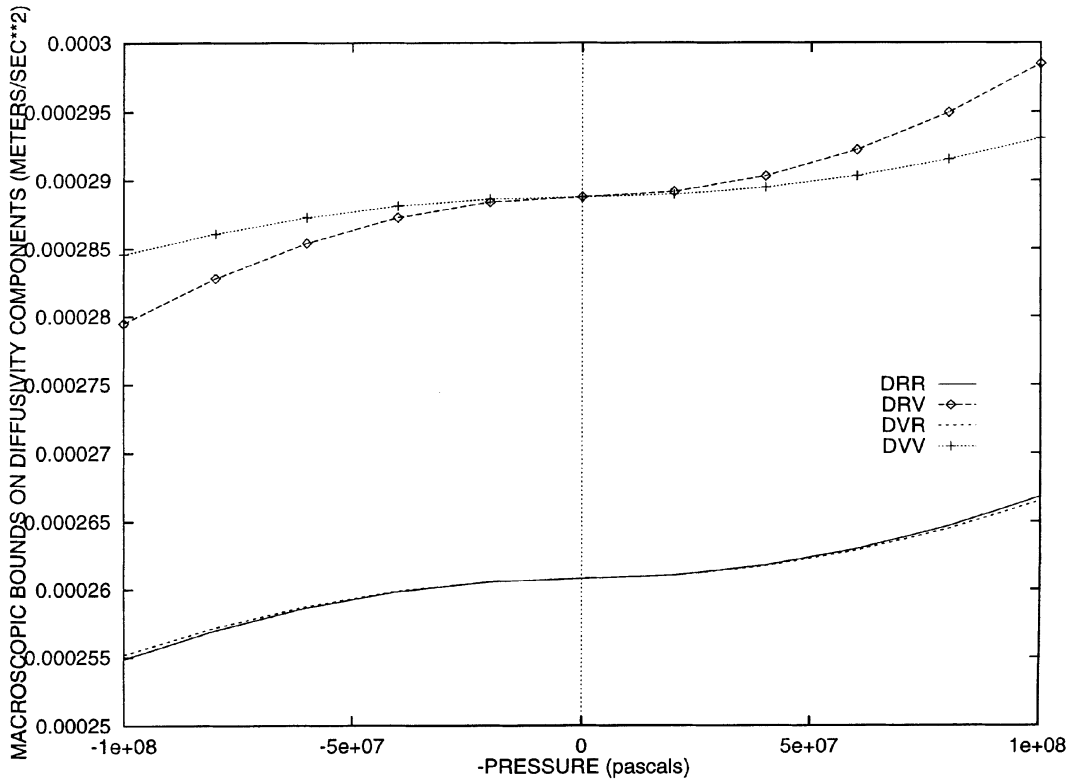
Fig. 17. 72.6%-ALUMINUM/27.4%-TITANIUM CARBIDE: The behavior of the effective diffusivity tensor components with pressure. The diffusive Reuss/Voigt bounds for the Reuss and Voigt pressure constructions. $DRR \stackrel{\text{def}}{=} \langle (D^{\sigma R})^{-1} \rangle^{-1}$, $DRV \stackrel{\text{def}}{=} \langle D^{\sigma R} \rangle$, $DVR \stackrel{\text{def}}{=} \langle (D^{\sigma V})^{-1} \rangle^{-1}$ and $DVV \stackrel{\text{def}}{=} \langle D^{\sigma V} \rangle$.

appropriate, due to the fact that more material variations can be captured by gauss points in the interior of each element, rather than with the nodally based finite difference method.

References

[1] D.C. Aifantis, New interpretation of diffusion in regions with high diffusivity paths: A continuum approach, Acta Metallurgica 27 (1979) 683–691.
[2] W.F. Ames, Numerical Methods for Partial Differential Equations, 2nd ed., Academic Press, New York, 1977.
[3] D.S. Chandrasekhariah, Thermoelasticity with second sound: A review, Appl. Mech. Reviews 39 (1986) 355–376.
[4] J. Crank, The mathematics of diffusion, 2nd ed., Oxford Science Publications, Oxford, 1975.
[5] P. Doig, T. Jones, A model for the initiation of hydrogen embrittlement cracking at notches in gaseous hydrogen environments, Metallurgical Transactions 18A (1977) 1993–1998.
[6] W. Dreyer, H. Struchtrup, Heat pulse experiments revisited, Cont. Mech. Thermodyn. 5 (1993) 13–50.
[7] W.W. Gerberich, T. Livine, X.F. Chen, M. Kaczorowski, Crack growth from hydrogen-temperature and microstructural effects in 4340 steel, Metallurgical Transactions 19A (1988) 1319–1334.
[8] W.W. Gerberich, T.J. Foecke, Hydrogen enhanced decohesion in Fe–Si single crystal: Implications to modeling thresholds in hydrogen effects on material behavior, in: N.R. Moody, A.W. Thompson (Eds), The Minerals, Metals and Materials Society, 1990.
[9] W.W. Gerberich, Hydrogen in metals. ASM, Metals Park, OH, 1974, p. 115.
[10] P. Haasen, Physical metallurgy, 2nd ed., Cambridge University Press, Cambridge, 1985.

[11] R. Hiil, The elastic behaviour of a crystalline aggregate, Proc. Phys. Soc. London A65 (1952) 349–354.

[12] R. Hill, Elastic properties of reinforced solids: Some theoretical principles, J. Mech. Phys. Solids. 11 (1963) 357–372.

[13] C. Huet, P. Navi, P.E. Roelfstra, A homogenization technique based on Hill's modification theorem, in: Continuum models and discrete systems, 1991.

[14] V.V. Jikov, S.M. Kozlov, O.A. Olenik, Homogenization of differential operators and integral functionals, Springer, Berlin, 1994.

[15] D.D. Joseph, L. Preziosi, Heat waves, Reviews of Modern Physics 61 (1) 1989.

[16] A. Mangeney, F. Califano, K. Hutter, A numerical study of anisotropic, low Reynolds number, free surface flow for ice sheet modeling, Journal of Geophysical Research 102 (10) (1997) 22749–22764.

[17] J.C. Maxwell, On the dynamical theory of gases, Philos. Trans. Soc. London 157 (1867) 49.

[18] I. Müller, T. Ruggeri, Extended thermodynamics, Springer, Berlin, 1993.

[19] J. Stark, Solid state diffusion, Krieger, New York, 1983.

[20] D.J. Unger, D.C. Aifantis, On the theory of stress-assisted diffusion, II, Acta Mechanica 47 (1983) 117–151.

[21] D.J. Unger, W.W. Gerberich, D.C. Aifantis, Further remarks on the implications of steady-state stress-assisted diffusion on environmental cracking, Scripta Metallurgica 16 (1982) 1059–1064.

[22] T.I. Zohdi, E.I. Meletis, On the intergranular hydrogen embrittlement mechanism of Al–Li alloys, Scripta Metallurgica 26 (1992) 1615–1620.

[23] T.I. Zohdi, P. Wriggers, On the effects of microstress on macroscopic diffusion processes. Acta Mechanica (in press).

[24] T.I. Zohdi, P. Wriggers, A methodology for large scale numerical simulation of the degradation of microheterogeneous solids, Computer Methods in Applied Mechanics and Engineering, submitted.